

Intrinsic superconducting diode effect and nonreciprocal superconductivity in rhombohedral graphene multilayers

Yinqi Chen, Constantin Schrade¹

¹*Hearne Institute of Theoretical Physics, Department of Physics & Astronomy,
Louisiana State University, Baton Rouge LA 70803, USA*

(Dated: March 21, 2025)

Rhombohedral tetralayer graphene has recently emerged as an exciting platform for a possible chiral superconducting state. Here, we theoretically demonstrate and study the emergence of nonreciprocal superconductivity and an intrinsic superconducting diode effect in this system. Our results are based on a fully self-consistent framework for determining the superconducting order parameter from a Kohn-Luttinger mechanism to superconductivity and show that large diode efficiencies, $\sim 60\%$, are achievable and highly tunable by an external displacement field. Moreover, we also find that the diodicity shows a characteristic angular dependence with multiple enhanced lobes, which depend on the Fermi surface structure of the underlying normal state. Hence, our results suggest that the intrinsic superconducting diode effect could provide insights into the type of Fermi surface topology from which superconductivity arises.

Non-reciprocal phenomena in superconducting systems that break time-reversal and inversion symmetry have recently attracted a great deal of attention [1]. A prominent example is the superconducting diode effect (SDE), characterized by a critical current that depends on the current-bias direction [2–8]. One established route to achieving such a SDE relies on applying an external magnetic field [9–18] or flux [19–26] to break time-reversal symmetry. However, it is also possible for certain materials to break the relevant symmetries at the microscopic level, giving rise to an *intrinsic* SDE [27–33]. Such an intrinsic SDE could enable field-free non-reciprocal circuit elements [34–39] and serve as a novel probe for symmetry-breaking in superconducting materials.

In an exciting recent development, superconductivity has been discovered in rhombohedral tetralayer graphene (RTLG) [40, 41]. A unique aspect of RTLG is that a superconducting phase can emerge from a spin- and valley-polarized “quarter-metal” parent state and persists under large in-plane magnetic fields [40]. These observations point to a possible spin-polarized pairing with a chiral $p + ip$ superconducting order parameter, as suggested by theoretical works [42–50]. Notably, both time-reversal symmetry (due to the quarter-metal normal state and chiral superconductivity) and inversion symmetry (due to an applied displacement field and trigonal warping) can be broken in RTLG. These symmetry-breaking properties make RTLG a promising platform for non-reciprocal superconducting phenomena. Indeed, an observation of an intrinsic SDE in RTLG has recently been reported [40].

Here, we theoretically demonstrate and study the emergence of nonreciprocal superconductivity, characterized by an asymmetric quasiparticle dispersion, and an intrinsic SDE in RTLG. Our results are based on a fully self-consistent framework for determining the superconducting order parameter from a Kohn-Luttinger mechanism to superconductivity and show that large diode efficiencies, $\sim 60\%$, are achievable and highly tunable by

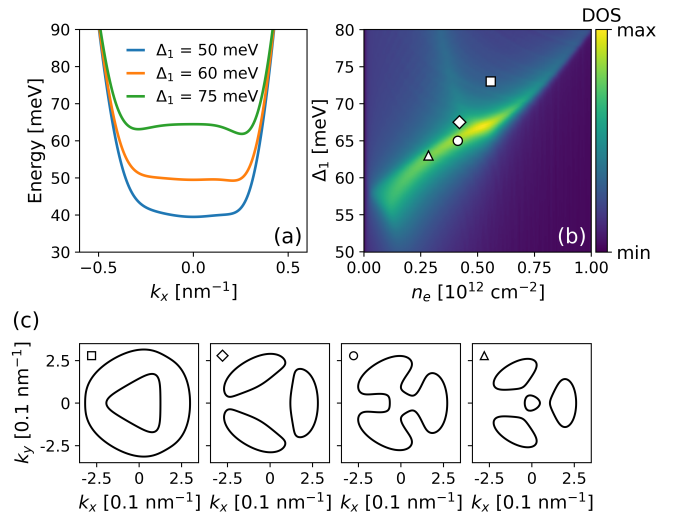


FIG. 1. (a) Dispersion of RTLG along the k_x -direction for different displacement fields, Δ_1 , showing a band flattening around $k_x = 0$. (b) Density of states (DOS) of RTLG as a function of Δ_1 and the carrier density, n_e (relative to the charge neutrality point), showing a significant enhancement due to the band flattening. (c) Fermi surfaces for (Δ_1, n_e) , from left to right, set to (72 meV, 0.574), (67.5 meV, 0.386), (65 meV, 0.414), (63 meV, 0.254).

an external displacement field. Moreover, we also find that the diodicity shows a characteristic angular dependence with multiple enhanced lobes, which depend on the Fermi surface topology of the underlying normal state. Hence, our results suggest that the intrinsic SDE could provide insights into the type of Fermi surface topology from which superconductivity arises.

Model. We consider a minimal model for spin- and valley-polarized RTLG. The non-interacting part of the Hamiltonian, H_0 , for describing the band structure near the K or K' valley (labeled by $\tau = \pm$) is written in the basis $(A_1, B_1, A_2, B_2, A_3, B_3, A_4, B_4)$, where A_ℓ and B_ℓ

denote the sublattices of the ℓ^{th} layer. It is given by [51],

$$H_0 = \begin{pmatrix} D - \delta & v_0\pi^\dagger & v_4\pi^\dagger & v_3\pi & 0 & \frac{\gamma_2}{2} & 0 & 0 \\ v_0\pi & D & \gamma_1 & v_4\pi^\dagger & 0 & 0 & 0 & 0 \\ v_4\pi & \gamma_1 & \frac{D}{3} & v_0\pi^\dagger & v_4\pi^\dagger & v_3\pi & 0 & \frac{\gamma_2}{2} \\ v_3\pi^\dagger & v_4\pi & v_0\pi & \frac{D}{3} & \gamma_1 & v_4\pi^\dagger & 0 & 0 \\ 0 & 0 & v_4\pi & \gamma_1 & -\frac{D}{3} & v_0\pi^\dagger & v_4\pi^\dagger & v_3\pi \\ \frac{\gamma_2}{2} & 0 & v_3\pi^\dagger & v_4\pi & v_0\pi & -\frac{D}{3} & \gamma_1 & v_4\pi^\dagger \\ 0 & 0 & 0 & 0 & v_4\pi & \gamma_1 & \delta - D & v_0\pi^\dagger \\ 0 & 0 & \frac{\gamma_2}{2} & 0 & v_3\pi^\dagger & v_4\pi & v_0\pi & -D - \delta \end{pmatrix}, \quad (1)$$

where $\pi = \tau k_x + ik_y$ and the momentum $\mathbf{k} = (k_x, k_y)$ is measured relative to K or K' valley. The k_x -direction correspond to the Γ - K direction of the full momentum-space Hamiltonian, while the k_y -direction corresponds to the Γ - M direction. The parameters $v_j = \sqrt{3}a\gamma_j/2$ are given in terms of the graphene lattice constant, $a = 2.46\text{\AA}$, and the hoppings, γ_j . Moreover, δ is a sublattice potential and D is an external displacement field. For our simulations, we use $(\gamma_0, \gamma_1, \gamma_2, \gamma_3, \gamma_4, \delta) = (3.1, 0.38, -0.015, -0.29, -0.141, -0.0105) \text{ eV}$ [52].

Diagonalizing H_0 in Eq. (1) shows that the low-energy conduction and valence bands in RTLG originate primarily from the weakly-coupled A_1 and B_4 sublattices. These sublattices of the top and bottom layers are only weakly coupled by interlayer hopping, resulting in low-energy bands that touch near the K or K' valley. The application of a displacement field, Δ_1 , opens an energy gap and flattens these lowest bands, leading to a significant enhancement of the density of states, see Fig. 1(a) and (b). Furthermore, a finite Δ_1 reverses the band curvature near $\mathbf{k} = 0$. As a result, the Fermi surface can display multiple connected components depending on Δ_1 and the electron density n_e , see Fig. 1(c).

The aforementioned flattening of the low-energy bands in RTLG enhances the importance of interaction effects. In the recent observation of superconductivity from a spin- and valley-polarized ‘‘quarter-metal’’, the chemical potential was tuned to the bottom of the lowest conduction band [40]. This motivates us to introduce the following effective Hamiltonian for the interacting system,

$$H_{\text{eff}} = \sum_{\mathbf{k}} \varepsilon_{\mathbf{k}} c_{\mathbf{k}}^\dagger c_{\mathbf{k}} + \frac{1}{2\Omega} \sum_{\mathbf{k}, \mathbf{k}', \mathbf{q}} \tilde{V}_{\mathbf{q}} F_{\mathbf{k}, \mathbf{k}+\mathbf{q}} F_{\mathbf{k}', \mathbf{k}'-\mathbf{q}} c_{\mathbf{k}}^\dagger c_{\mathbf{k}+\mathbf{q}} c_{\mathbf{k}'}^\dagger c_{\mathbf{k}'-\mathbf{q}} \quad (2)$$

The first term describes the dispersion, $\varepsilon_{\mathbf{k}}$, of the lowest conduction band obtained from H_0 with $c_{\mathbf{k}}$ denoting the electron annihilation operator of that band.

The second term captures interaction effects by projecting a repulsive Coulomb interaction onto the lowest conduction band and accounting for screening effects at the level of the random phase approximation (RPA). This projection introduces the structure factors,

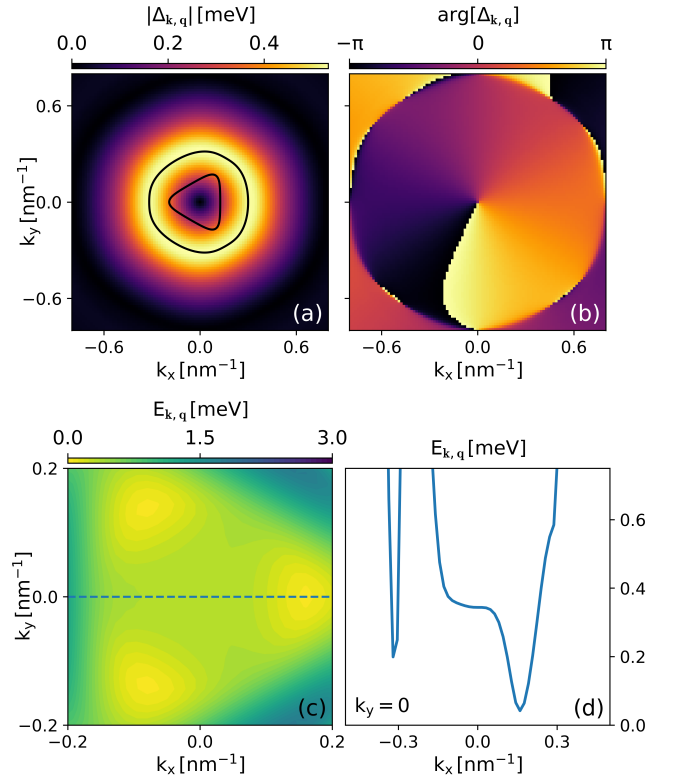


FIG. 2. (a) Magnitude of the superconducting order parameter, $\Delta_{\mathbf{k},\mathbf{q}}$, for the Fermi surface shown as an inset in the zero-temperature limit. (b) Phase of the superconducting order parameter, showing a $p + ip$ winding. (c) Quasiparticle dispersion, $E_{\mathbf{k},\mathbf{q}}$, associated with the superconducting order parameter shown in (a) and (b). (d) The quasiparticle dispersion is asymmetric under $k_x \rightarrow -k_x$. Hence, RTLG realizes a nonreciprocal superconductor.

$F_{\mathbf{k}, \mathbf{k}+\mathbf{q}} = \langle \psi_{\mathbf{k}} | \psi_{\mathbf{k}+\mathbf{q}} \rangle$, that describe the overlap of Bloch states in the lowest conduction band. Moreover, the RPA-screened Coulomb potential is,

$$\tilde{V}_{\mathbf{q}} = \frac{V_{\mathbf{q}}}{1 - \Pi_{\mathbf{q}} V_{\mathbf{q}}}. \quad (3)$$

where $V_{\mathbf{q}} = \frac{e^2}{2\epsilon} \frac{\tanh(|\mathbf{q}|d)}{|\mathbf{q}|}$ denotes the gate-screened Coulomb potential with d being the distance to the metallic gates and ϵ the dielectric permittivity of the hexagonal boron nitride encapsulation. We take $d = 20 \text{ nm}$ and $\epsilon = 6\epsilon_0$ with ϵ_0 the vacuum permittivity. The polarization function, $\Pi_{\mathbf{q}}$, entering Eq. (3) is given by, $\Pi_{\mathbf{q}} = \frac{1}{\Omega} \sum_{\mathbf{k}} \frac{n_F(\varepsilon_{\mathbf{k}+\mathbf{q}}) - n_F(\varepsilon_{\mathbf{k}})}{\varepsilon_{\mathbf{k}+\mathbf{q}} - \varepsilon_{\mathbf{k}}} |F_{\mathbf{k}, \mathbf{k}+\mathbf{q}}|^2$, where n_F is the Fermi-Dirac distribution and Ω the area of the system.

We will now use this effective Hamiltonian to explain the emergence of nonreciprocal superconductivity and an intrinsic SDE in RTLG.

Nonreciprocal superconductivity. We begin by discussing the emergence of nonreciprocal superconductivity. Nonreciprocal superconductors are a recently proposed class of superconductors in which the breaking of

time-reversal and inversion symmetry leads to an asymmetric quasiparticle dispersion [53]. A possible mechanism for such nonreciprocity is finite-momentum pairing. However, as noted in previous works, the Cooper-pair momentum \mathbf{q} (defined relative to the K or K' valley) in RTLG can be small [44, 45]. We will now explicitly show that the primary origin of the asymmetric quasiparticle dispersion in RTLG is the intrinsic asymmetry of the normal-state band structure, $\varepsilon_{\mathbf{k}} \neq \varepsilon_{-\mathbf{k}}$. Nevertheless, a finite Cooper-pair momentum can still *qualitatively* modify the symmetry properties of the quasiparticle dispersion.

To describe the superconductivity in RTLG, we consider, inspired by earlier works [42–47], a Kohn-Luttinger mechanisms [51, 54–57]. Specifically, while the bare Coulomb potential, $V_{\mathbf{q}}$, is nominally repulsive, the screening effects described by Eq. (3) can lead to an “over-screening” regime, where the effective interaction becomes attractive. This effective attraction can be verified by transforming $\tilde{V}_{\mathbf{q}}$ to real space.

We will assume that this effective attraction can lead to pairing between momentum states $\mathbf{k} + \frac{\mathbf{q}}{2}$ and $-\mathbf{k} + \frac{\mathbf{q}}{2}$ where \mathbf{q} is the Cooper-pair momentum. While we retain the possibility of a finite \mathbf{q} , we emphasize that it is not a necessary ingredient for the nonreciprocal superconductivity and SDE. We then perform a mean-field decoupling of the interaction in Eq. (2) in the Cooper channel. The superconducting order parameter is determined self-consistently as,

$$\Delta_{\mathbf{k},\mathbf{q}} = - \sum_{\mathbf{k}'} g_{\mathbf{k},\mathbf{k}',\mathbf{q}} \frac{\Delta_{\mathbf{k}',\mathbf{q}}}{2\tilde{E}_{\mathbf{k}',\mathbf{q}}} \times \frac{1}{2} \left\{ \tanh\left(\frac{\beta E_{\mathbf{k}',\mathbf{q}}}{2}\right) + \tanh\left(\frac{\beta E_{-\mathbf{k}',\mathbf{q}}}{2}\right) \right\}. \quad (4)$$

where $g_{\mathbf{k},\mathbf{k}',\mathbf{q}} = \tilde{V}_{\mathbf{k}'-\mathbf{k}} F_{\mathbf{k}+\frac{\mathbf{q}}{2},\mathbf{k}'+\frac{\mathbf{q}}{2}} F_{-\mathbf{k}+\frac{\mathbf{q}}{2},-\mathbf{k}'+\frac{\mathbf{q}}{2}}$ is the pairing interaction, $1/\beta = k_B T$, and the quasiparticle dispersion is given by,

$$E_{\mathbf{k},\mathbf{q}} = \xi_{\mathbf{k},\mathbf{q},-} + \sqrt{(\xi_{\mathbf{k},\mathbf{q},+})^2 + |\Delta_{\mathbf{k},\mathbf{q}}|^2} \quad (5)$$

Here, we have defined the symmetric and antisymmetric components of the normal-state dispersion as $\xi_{\mathbf{k},\mathbf{q},\pm} = (\varepsilon_{\mathbf{k}+\frac{\mathbf{q}}{2}} \pm \varepsilon_{-\mathbf{k}+\frac{\mathbf{q}}{2}})/2$. Moreover, we have introduced the reduced quasiparticle dispersion, $\tilde{E}_{\mathbf{k}',\mathbf{q}} = E_{\mathbf{k},\mathbf{q}} - \xi_{\mathbf{k},\mathbf{q},-}$.

Next, we solve for $\Delta_{\mathbf{k},\mathbf{q}}$ self-consistently, imposing a fixed electron density $n_e = \sum_{\mathbf{k}} \langle c_{\mathbf{k}}^\dagger c_{\mathbf{k}} \rangle / \Omega$ and varying \mathbf{q} . The realized superconducting order, $\Delta_{\mathbf{k},\mathbf{q}}$, is determined by minimizing the free energy,

$$F = - \sum_{\mathbf{k}} \left\{ \frac{1}{\beta} \ln(1 + e^{-\beta E_{\mathbf{k},\mathbf{q}}}) - \frac{1}{2} (\xi_{\mathbf{k},\mathbf{q},+} - \tilde{E}_{\mathbf{k},\mathbf{q}}) - \frac{|\Delta_{\mathbf{k},\mathbf{q}}|^2}{8\tilde{E}_{\mathbf{k},\mathbf{q}}} \left[\tanh\left(\frac{\beta E_{\mathbf{k},\mathbf{q}}}{2}\right) + \tanh\left(\frac{\beta E_{-\mathbf{k},\mathbf{q}}}{2}\right) \right] \right\} \quad (6)$$

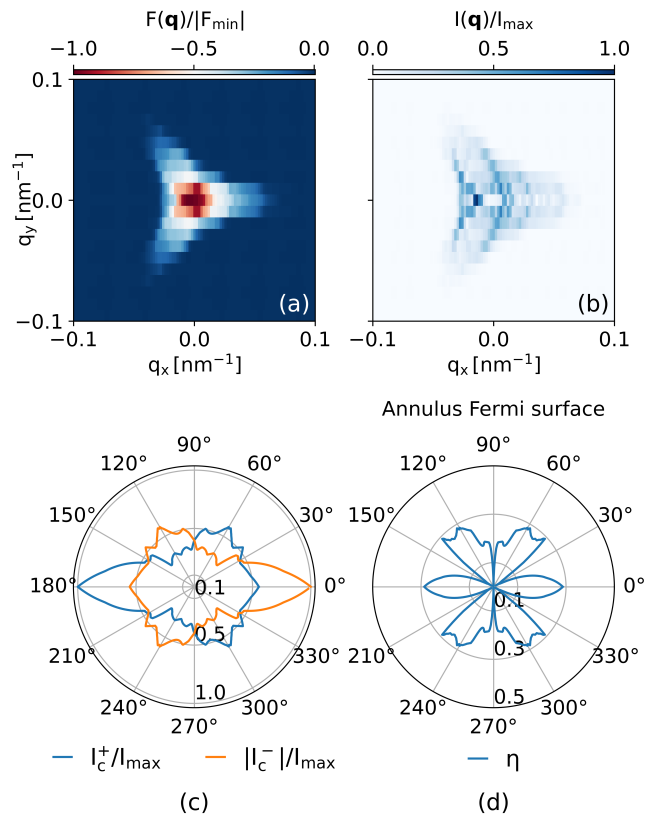


FIG. 3. (a) Free energy, F , versus $\mathbf{q} = (q_x, q_y)$ for the annulus Fermi surface shown in Fig. 2. Here, $F_{\min} \equiv \min_{\mathbf{q}}\{F(\mathbf{q})\}$. (b) Corresponding supercurrent magnitude, I , as a function of \mathbf{q} . Here, $I_{\max} \equiv \max_{\mathbf{q}}\{I(\mathbf{q})\}$. (c) Critical currents in the forward direction ($I_{c,+}$) and reverse direction ($I_{c,-}$) for current direction given by an angle θ relative to the x -direction. (d) Diode efficiency for a current direction given by an angle θ .

An example result of self-consistency calculation is shown in Fig. 2(a) and (b) for a Fermi surface with an annulus topology. We see that the superconducting order parameter exhibits a $p + ip$ phase winding. The Cooper-pair momentum is found to be small but finite ($q_0 = -0.004 \text{ nm}^{-1}$), oriented along the q_x -direction (i.e., the Γ - K direction). Using the self-consistent solution, we then compute the quasiparticle dispersion, $E_{\mathbf{k},\mathbf{q}}$, see Fig. 2(c). The quasiparticle dispersion is in general found to be asymmetric with respect to $\mathbf{k} \rightarrow -\mathbf{k}$. Hence, RTLG realizes nonreciprocal superconductivity. Writing $\mathbf{k} = (k \cos \theta, k \sin \theta)$, we see that the asymmetry is most pronounced along $\theta \in \{0^\circ, 60^\circ, 120^\circ\}$. It is instructive to discuss these results from a symmetry perspective.

First, we assume $\mathbf{q} = 0$. The normal state spectrum is invariant under two three-fold rotations ($2C_3$) and three two-fold rotations ($3C_2'$) around the in-plane axis pointing along $\theta \in \{0^\circ, 60^\circ, 120^\circ\}$. Consider a \mathbf{k} pointing along one of the directions $\theta \in \{90^\circ, 150^\circ, 30^\circ\}$. Then, $C_2' \mathbf{k} = -\mathbf{k}$ and hence $\varepsilon_{-\mathbf{k}} = \varepsilon_{C_2' \mathbf{k}} = \varepsilon_{\mathbf{k}}$. As a result,

$\xi_{\mathbf{k},\mathbf{q},-} = 0$ and $E_{\mathbf{k},\mathbf{q}} = E_{-\mathbf{k},\mathbf{Q}}$ (since $|\Delta_{\mathbf{k},\mathbf{q}}| = |\Delta_{-\mathbf{k},\mathbf{q}}|$). Consequently, if $\mathbf{q} = 0$, the quasiparticle spectrum is symmetric along the directions $\theta \in \{90^\circ, 150^\circ, 30^\circ\}$, but asymmetric otherwise.

Now assume $\mathbf{q} \neq 0$. In this case, a vanishing asymmetry of the quasiparticle spectrum requires both $C'_2 \mathbf{k} = -\mathbf{k}$ and $C'_2 \mathbf{q} = \mathbf{q}$. In our simulations, we found that \mathbf{q} typically pointed along the $\theta = 0^\circ$ directions so that the two conditions can only be satisfied for momenta \mathbf{k} with $\theta = 90^\circ$. Consequently, the quasiparticle dispersion can be strictly symmetric only along $\theta = 90^\circ$; in all other directions, it remains asymmetric.

One experimental manifestation of the asymmetric quasiparticle dispersion is that a transparent normal-metal-superconductor junction can exhibit a current-voltage (I - V) characteristic that is not invariant under $V \rightarrow -V$ [53]. Our results suggest the following probe of the nonreciprocal superconductivity in RTLG: connect two normal leads to the RTLG superconductor, one along $\theta = 0^\circ$ (Γ - K direction) and one along $\theta = 90^\circ$ (Γ - M direction). Our results imply that the lead along $\theta = 0^\circ$ would show an asymmetric I - V curve, while the I - V curve along $\theta = 90^\circ$ would remain symmetric.

Intrinsic SDE. We are now in the position to evaluate the SDE for RTLG. For this purpose, we self-consistently solve for the superconducting order parameter for a broader range of Cooper-pair momenta, \mathbf{q} , and use the obtained $\Delta_{\mathbf{k},\mathbf{q}}$ to evaluate the free energy. The results of the free energy are shown in Fig. 3(a). The current in the ground state that minimizes $F(\mathbf{q})$ is always zero. However, applying a finite current-bias, produces a state with a finite Cooper-pair momentum different from the ground state value, $\mathbf{q} \neq \mathbf{q}_0$. The current in this state is $I = (2e/\hbar)|\partial_{\mathbf{q}}F(\mathbf{q})|$ [13].

As a next step, we compute the supercurrent versus \mathbf{q} are shown in Fig. 3(b). Upon fixing a direction, θ , so that $\mathbf{q} = (q \cos \theta, q \sin \theta)$, this allows us to determine the critical current in the forward direction, $I_{c,+} \equiv \max_{q>0}\{I(q, \theta)\}$ and in the reversed direction as, $I_{c,-} \equiv \max_{q>0}\{I(q, \theta + \pi)\}$. The diode efficiency is then defined as,

$$\eta = \frac{|I_c^+ - I_c^-|}{I_c^+ + I_c^-}. \quad (7)$$

Here, we defined η as non-negative. However, we remark that the modified efficiency $\eta_{\text{signed}} = \frac{I_c^+ - I_c^-}{I_c^+ + I_c^-}$ can exhibit sign changes when transitioning through $\eta = 0$ [58].

We begin by evaluating the angular dependence of the critical currents and diode efficiencies for fixed Δ_1 and n_e . Our results are shown in Fig. 3(c) and (d) for a Fermi surface with annulus topology. We find that, in general, the diode efficiency takes on finite values. This verifies the emergence of an intrinsic SDE from a fully self-consistent calculation. Furthermore, we find that η exhibits a characteristic multi-lobe structure. Specifically, we see that

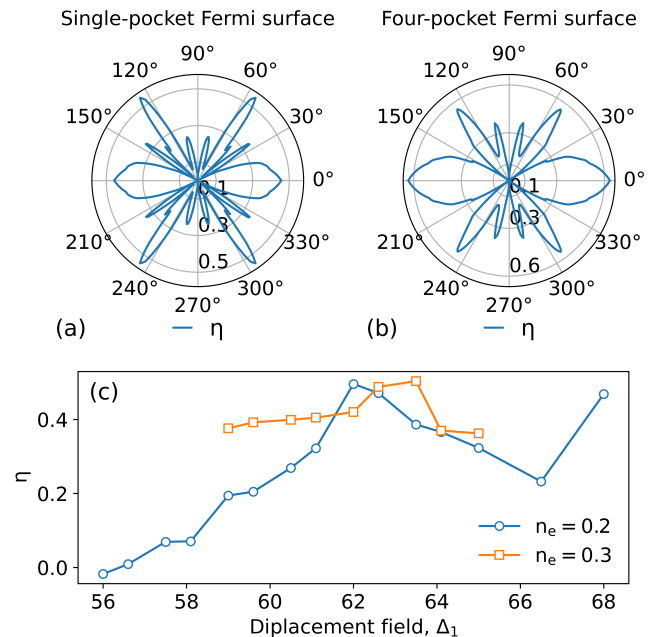


FIG. 4. (a) Angular dependence of the diode efficiency, η , for the single-pocket Fermi surface shown in Fig. 1(c). (b) Same as (a) but for the four-pocket Fermi surface shown in Fig. 1(c). (c) Diode efficiency, η , versus the displacement field along the q_x direction for different electron densities, n_e .

the efficiency tends to be maximized along the directions $\theta \in \{0^\circ, 60^\circ, 120^\circ\}$, reaching values of $\sim 30\%$ for the annulus Fermi surface. In addition, it is strongly suppressed along the directions $\theta \in \{30^\circ, 90^\circ, 150^\circ\}$. Moreover, the efficiency in the $\theta = 0^\circ, 90^\circ$ lobes is functionally different from the remaining lobes. We attribute this difference to the small but finite Cooper-pair momentum along q_x .

It is now interesting to compare these results for the annulus Fermi surface with other Fermi surface topologies. Our results for a single-pocket Fermi surface and a four-pocket Fermi surface are shown in Fig. 4(a) and (b). We see that the shape of the lobes changes qualitatively. Specifically, the width of the lobes around $\theta \in \{60^\circ, 120^\circ\}$ is significantly reduced. Furthermore, in these lobes, the maximum efficiency is achieved slightly away from $\theta = 60^\circ, 120^\circ$. The overall highest efficiency is found for the four-pocket Fermi surface at $\sim 60\%$. These results suggest that the Fermi surface topology can affect the angular dependence of the diode efficiency and, as a result, could provide insights into the type of Fermi surface topology from which the superconducting state arises. We provide more detailed plots of the free energies and critical currents for single-pocket and four-pocket Fermi surface in the Supplemental Material [58].

Finally, we have also investigated the diode efficiency as a function of the displacement field, Δ_1 , for different densities, n_e , and along the fixed q_x -direction. Our results are shown in Fig. 4(c). We find that, in general,

that the diode efficiency seems to increase with increasing displacement field. However, we remark that the system can enter a metallic phase if the displacement field is increased beyond a density-dependent threshold.

Conclusion. In this work, we have theoretically demonstrated and studied the emergence of an intrinsic SDE and non-reciprocal superconductivity in RTLG through a fully self-consistent approach to determining the superconducting order parameter. Our results suggest that angular dependence of the diodicity in RTLG could provide insights into the type of Fermi surface topology from which superconductivity arises.

Note added. We have recently become aware of a related work [50].

Acknowledgement. We acknowledge helpful discussions with Marco Valentini.

-
- [1] M. Nadeem, M. S. Fuhrer, and X. Wang, [The superconducting diode effect](#), *Nature Reviews Physics* **5**, 558 (2023).
- [2] F. Ando, Y. Miyasaka, T. Li, J. Ishizuka, T. Arakawa, Y. Shiota, T. Moriyama, Y. Yanase, and T. Ono, [Observation of superconducting diode effect](#), *Nature* **584**, 373 (2020).
- [3] J. J. He, Y. Tanaka, and N. Nagaosa, [A phenomenological theory of superconductor diodes](#), *New Journal of Physics* **24**, 053014 (2022).
- [4] N. F. Yuan and L. Fu, [Supercurrent diode effect and finite-momentum superconductors](#), *Proceedings of the National Academy of Sciences* **119**, e2119548119 (2022).
- [5] Y. Zhang, Y. Gu, P. Li, J. Hu, and K. Jiang, [General Theory of Josephson Diodes](#), *Physical Review X* **12**, 041013 (2022).
- [6] K. Misaki and N. Nagaosa, [Theory of the nonreciprocal Josephson effect](#), *Physical Review B* **103**, 245302 (2021).
- [7] M. Davydova, S. Prembabu, and L. Fu, [Universal Josephson diode effect](#), *Science advances* **8**, eabo0309 (2022).
- [8] R. S. Souto, M. Leijnse, C. Schrade, M. Valentini, G. Katsaros, and J. Danon, [Tuning the Josephson diode response with an ac current](#), *Physical Review Research* **6**, L022002 (2024).
- [9] A. Zazunov, R. Egger, T. Jonckheere, and T. Martin, [Anomalous Josephson current through a spin-orbit coupled quantum dot](#), *Physical Review Letters* **103**, 147004 (2009).
- [10] A. Brunetti, A. Zazunov, A. Kundu, and R. Egger, [Anomalous Josephson current, incipient time-reversal symmetry breaking, and Majorana bound states in interacting multilevel dots](#), *Physical Review B* **88**, 144515 (2013).
- [11] B. Pal, A. Chakraborty, P. K. Sivakumar, M. Davydova, A. K. Gopi, A. K. Pandeya, J. A. Krieger, Y. Zhang, M. Date, S. Ju, et al., [Josephson diode effect from Cooper pair momentum in a topological semimetal](#), *Nature Physics* **18**, 1228 (2022).
- [12] C. Baumgartner, L. Fuchs, A. Costa, S. Reinhardt, S. Gronin, G. C. Gardner, T. Lindemann, M. J. Manfra, P. E. Faria Junior, D. Kochan, et al., [Supercurrent rectification and magnetochiral effects in symmetric Josephson junctions](#), *Nature Nanotechnology* **17**, 39 (2022).
- [13] H. F. Legg, D. Loss, and J. Klinovaja, [Superconducting diode effect due to magnetochiral anisotropy in topological insulators and Rashba nanowires](#), *Physical Review B* **106**, 104501 (2022).
- [14] N. Lotfizadeh, W. F. Schiela, B. Pekerten, P. Yu, B. H. Elfeky, W. M. Strickland, A. Matos-Abiague, and J. Shabani, [Superconducting diode effect sign change in epitaxial Al-InAs Josephson junctions](#), *Communications Physics* **7**, 120 (2024).
- [15] A. Costa, J. Fabian, and D. Kochan, [Microscopic study of the Josephson supercurrent diode effect in Josephson junctions based on two-dimensional electron gas](#), *Physical Review B* **108**, 054522 (2023).
- [16] A. Maiani, K. Flensberg, M. Leijnse, C. Schrade, S. Vaitiekėnas, and R. S. Souto, [Nonsinusoidal current-phase relations in semiconductor–superconductor–ferromagnetic insulator devices](#), *Physical Review B* **107**, 245415 (2023).
- [17] R. Hess, H. F. Legg, D. Loss, and J. Klinovaja, [Josephson transistor from the superconducting diode effect in domain wall and skyrmion magnetic racetracks](#), *Physical Review B* **108**, 174516 (2023).
- [18] Y. Hou, F. Nichele, H. Chi, A. Lodesani, Y. Wu, M. F. Ritter, D. Z. Haxell, M. Davydova, S. Ilić, O. Glezakou-Elbert, et al., [Ubiquitous superconducting diode effect in superconductor thin films](#), *Physical Review Letters* **131**, 027001 (2023).
- [19] A. Kononov, G. Abulizi, K. Qu, J. Yan, D. Mandrus, K. Watanabe, T. Taniguchi, and C. Schönberger, [One-dimensional edge transport in few-layer WTe₂](#), *Nano letters* **20**, 4228 (2020).
- [20] R. S. Souto, M. Leijnse, and C. Schrade, [Josephson Diode Effect in Supercurrent Interferometers](#), *Physical Review Letters* **129**, 267702 (2022).
- [21] M. Gupta, G. V. Graziano, M. Pendharkar, J. T. Dong, C. P. Dempsey, C. Palmstrøm, and V. S. Pribiag, [Gate-tunable superconducting diode effect in a three-terminal Josephson device](#), *Nature Communications* **14**, 3078 (2023).
- [22] C. Ciaccia, R. Haller, A. C. C. Drachmann, T. Lindemann, M. J. Manfra, C. Schrade, and C. Schönberger, [Gate-tunable Josephson diode in proximitized InAs supercurrent interferometers](#), *Phys. Rev. Res.* **5**, 033131 (2023).
- [23] M. Valentini, O. Sagi, L. Baghumyan, T. de Gijssel, J. Jung, S. Calcaterra, A. Ballabio, J. Aguilera Servin, K. Aggarwal, M. Janik, et al., [Parity-conserving Cooper-pair transport and ideal superconducting diode in planar germanium](#), *Nature Communications* **15**, 169 (2024).
- [24] A. Greco, Q. Pichard, and F. Giazotto, [Josephson diode effect in monolithic dc-SQUIDs based on 3D Dayem nanobridges](#), *Applied Physics Letters* **123** (2023).
- [25] H. F. Legg, K. Laubscher, D. Loss, and J. Klinovaja, [Parity-protected superconducting diode effect in topological Josephson junctions](#), *Physical Review B* **108**, 214520 (2023).
- [26] J. J. Cuozzo, W. Pan, J. Shabani, and E. Rossi, [Microwave-tunable diode effect in asymmetric SQUIDs with topological Josephson junctions](#), *Physical Review Research* **6**, 023011 (2024).
- [27] A. Daido, Y. Ikeda, and Y. Yanase, [Intrinsic superconducting diode effect](#), *Physical Review Letters* **128**,

- 037001 (2022).
- [28] H. Wu, Y. Wang, Y. Xu, P. K. Sivakumar, C. Pasco, U. Filippozzi, S. S. P. Parkin, Y.-J. Zeng, T. McQueen, and M. N. Ali, [The field-free Josephson diode in a van der Waals heterostructure](#), *Nature* **604**, 653 (2022).
- [29] N. J. Zhang, J.-X. Lin, D. V. Chichinadze, Y. Wang, K. Watanabe, T. Taniguchi, L. Fu, and J. Li, [Angle-resolved transport non-reciprocity and spontaneous symmetry breaking in twisted trilayer graphene](#), *Nature Materials* **23**, 356 (2024).
- [30] H. D. Scammell, J. Li, and M. S. Scheurer, [Theory of zero-field superconducting diode effect in twisted trilayer graphene](#), *2D Materials* **9**, 025027 (2022).
- [31] S. Banerjee and M. S. Scheurer, [Enhanced superconducting diode effect due to coexisting phases](#), *Phys. Rev. Lett.* **132**, 046003 (2024).
- [32] J. Díez-Mérida, A. Díez-Carlón, S. Yang, Y.-M. Xie, X.-J. Gao, J. Senior, K. Watanabe, T. Taniguchi, X. Lu, A. P. Higginbotham, et al., [Symmetry-broken Josephson junctions and superconducting diodes in magic-angle twisted bilayer graphene](#), *Nature Communications* **14**, 2396 (2023).
- [33] J.-X. Hu, Z.-T. Sun, Y.-M. Xie, and K. T. Law, [Josephson Diode Effect Induced by Valley Polarization in Twisted Bilayer Graphene](#), *Physical Review Letters* **130**, 266003 (2023).
- [34] M. Khabipov, V. Gaydamachenko, C. Kissling, R. Dolata, and A. Zorin, [Superconducting microwave resonators with non-centrosymmetric nonlinearity](#), *Superconductor Science and Technology* **35**, 065020 (2022).
- [35] N. E. Frattini, U. Vool, S. Shankar, A. Narla, K. M. Sliwa, and M. H. Devoret, [3-wave mixing Josephson dipole element](#), *Applied Physics Letters* **110**, 222603 (2017).
- [36] N. Frattini, V. Sivak, A. Lingenfelter, S. Shankar, and M. Devoret, [Optimizing the nonlinearity and dissipation of a snail parametric amplifier for dynamic range](#), *Physical Review Applied* **10**, 054020 (2018).
- [37] V. Sivak, N. Frattini, V. Joshi, A. Lingenfelter, S. Shankar, and M. Devoret, [Kerr-Free Three-Wave Mixing in Superconducting Quantum Circuits](#), *Physical Review Applied* **11**, 054060 (2019).
- [38] A. Miano, G. Liu, V. V. Sivak, N. E. Frattini, V. R. Joshi, W. Dai, L. Frunzio, and M. H. Devoret, [Frequency-tunable Kerr-free three-wave mixing with a gradiometric SNAIL](#), *Applied Physics Letters* **120**, 184002 (2022).
- [39] C. Schrade and V. Fatemi, [Dissipationless nonlinearity in quantum material josephson diodes](#), *Phys. Rev. Appl.* **21**, 064029 (2024).
- [40] T. Han, Z. Lu, Z. Hadjri, L. Shi, Z. Wu, W. Xu, Y. Yao, A. A. Cotten, O. S. Sedeh, H. Weldeyesus, et al., [Signatures of chiral superconductivity in rhombohedral graphene](#), arXiv preprint [arXiv:2408.15233](#) (2024).
- [41] Y. Choi, Y. Choi, M. Valentini, C. L. Patterson, L. F. W. Holleis, O. I. Sheekey, H. Stoyanov, X. Cheng, T. Taniguchi, K. Watanabe, et al., [Electric field control of superconductivity and quantized anomalous hall effects in rhombohedral tetralayer graphene](#), arXiv preprint [arXiv:2408.12584](#) (2024).
- [42] M. Geier, M. Davydova, and L. Fu, [Chiral and topological superconductivity in isospin polarized multilayer graphene](#), arXiv preprint [arXiv:2409.13829](#) (2024).
- [43] Y.-Z. Chou, J. Zhu, and S. D. Sarma, [Intravalley spin-polarized superconductivity in rhombohedral tetralayer graphene](#), arXiv preprint [arXiv:2409.06701](#) (2024).
- [44] H. Yang and Y.-H. Zhang, [Topological incommensurate fulde-ferrell-larkin-ovchinnikov superconductor and bogoliubov fermi surface in rhombohedral tetra-layer graphene](#), arXiv preprint [arXiv:2411.02503](#) (2024).
- [45] Q. Qin and C. Wu, [Chiral finite-momentum superconductivity in the tetralayer graphene](#), arXiv preprint [arXiv:2412.07145](#) (2024).
- [46] G. Parra-Martinez, A. Jimeno-Pozo, V. T. Phong, H. Sainz-Cruz, D. Kaplan, P. Emanuel, Y. Oreg, P. A. Pantaleón, J. A. Silva-Guillén, and F. Guinea, [Band renormalization, quarter metals, and chiral superconductivity in rhombohedral tetralayer graphene](#), arXiv preprint [arXiv:2502.19474](#) (2025).
- [47] Z. Dong and P. A. Lee, [A controllable theory of superconductivity due to strong repulsion in a polarized band](#) (2025), 2503.11079.
- [48] A. Jahin and S.-Z. Lin, [Enhanced kohn-luttinger topological superconductivity in bands with nontrivial geometry](#), arXiv preprint [arXiv:2411.09664](#) (2024).
- [49] Y.-Q. Wang, Z.-Q. Gao, and H. Yang, [Chiral superconductivity from parent chern band and its non-abelian generalization](#), arXiv preprint [arXiv:2410.05384](#) (2024).
- [50] C. Yoon, T. Xu, Y. Barlas, and F. Zhang, [Quarter metal superconductivity](#), arXiv preprint [arXiv:2502.17555](#) (2025).
- [51] A. Ghazaryan, T. Holder, E. Berg, and M. Serbyn, [Multilayer graphenes as a platform for interaction-driven physics and topological superconductivity](#), *Phys. Rev. B* **107**, 104502 (2023).
- [52] H. Zhou, T. Xie, A. Ghazaryan, T. Holder, J. R. Ehrets, E. M. Spanton, T. Taniguchi, K. Watanabe, E. Berg, M. Serbyn, et al., [Half-and quarter-metals in rhombohedral trilayer graphene](#), *Nature* **598**, 429 (2021).
- [53] M. Davydova, M. Geier, and L. Fu, [Nonreciprocal superconductivity](#), *Science Advances* **10**, eadr4817 (2024), <https://www.science.org/doi/pdf/10.1126/sciadv.adr4817>.
- [54] W. Kohn and J. Luttinger, [New mechanism for superconductivity](#), *Physical Review Letters* **15**, 524 (1965).
- [55] A. V. Chubukov, [Kohn-luttinger effect and the instability of a two-dimensional repulsive fermi liquid at \$t=0\$](#) , *Physical Review B* **48**, 1097 (1993).
- [56] A. Ghazaryan, T. Holder, M. Serbyn, and E. Berg, [Unconventional superconductivity in systems with annular fermi surfaces: Application to rhombohedral trilayer graphene](#), *Phys. Rev. Lett.* **127**, 247001 (2021).
- [57] C. Schrade and L. Fu, [Nematic, chiral, and topological superconductivity in twisted transition metal dichalcogenides](#), *Phys. Rev. B* **110**, 035143 (2024).
- [58] In the Supplemental Material, we provide details on the angular dependence of the diode efficiency and the the mean-field approach for describing the superconducting RTL system.

Supplemental Material to ‘Intrinsic superconducting diode effect and nonreciprocal superconductivity in rhombohedral graphene multilayers’

Yinqi Chen, Constantin Schrade¹

¹*Hearne Institute of Theoretical Physics, Department of Physics & Astronomy, Louisiana State University, Baton Rouge LA 70803, USA*

In the Supplemental Material, we provide details on the angular dependence of the diode efficiency and the the mean-field approach for describing the superconducting RTLГ system.

1. ANGULAR-DEPENDENCE OF THE DIODE EFFICIENCY

In this first section of the Supplementary Material, we provide more details on the angular dependence of the diode efficiency for different Fermi surfaces. We also suggest a possible experimental setup to probe the angular dependence of the diodicity.

Specifically, the obtained angular dependence of the diodicity for a single-pocket Fermi surface and a four-pocket Fermi surface (as shown in Fig. 1(c) in the main text) are given in Fig. 5 and Fig. 6. We also show the signed diode efficiency, η_{signed} , for the annulus Fermi surface in Fig. 7.

To measure the angular dependence of the diode efficiency, we propose a possible experimental setup, which is schematically shown in Fig. 8 and inspired by [29]. In the proposed setup, a circular superconducting RTLГ

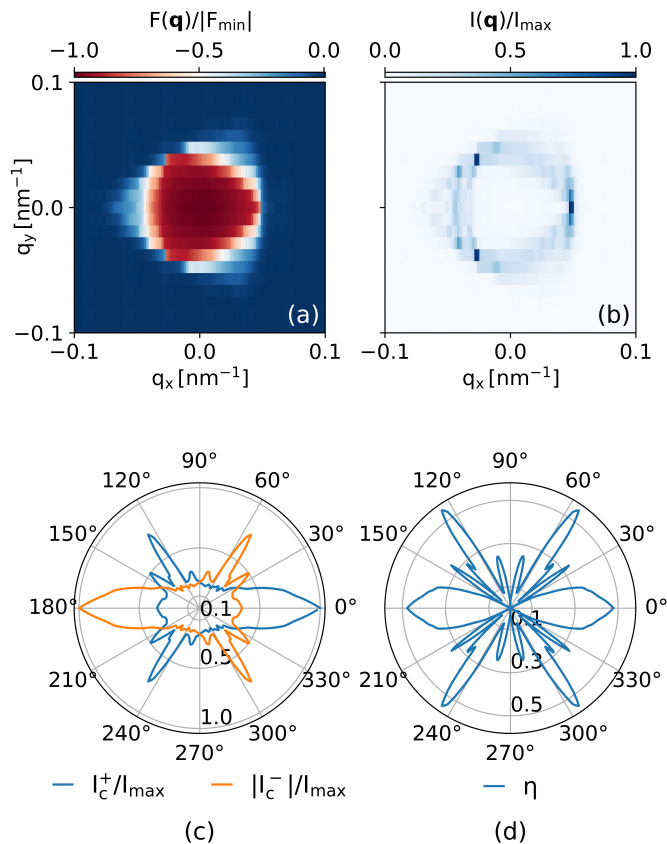


FIG. 5. Results for a Fermi surface with *one connected components* (as shown in Fig. 1(c) of the main text). (a) Free energy, F , as a function of $\mathbf{q} = (q_x, q_y)$. Here, $F_{\min} \equiv \min_{\mathbf{q}} F(\mathbf{q})$. (b) Corresponding supercurrent magnitude, I , as a function of \mathbf{q} . Here, $I_{\max} \equiv \max_{\mathbf{q}} I(\mathbf{q})$. (c) Critical currents in the forward direction ($I_{c,+}$) and reverse direction ($I_{c,-}$) for current direction given by an angle θ relative to the x -direction. (d) Diode efficiency for a current direction given by an angle θ .

system is connected to multiple leads. Applying a current-bias across the different possible directions would allow for a measurement of the critical currents and the diodicity along the different directions.

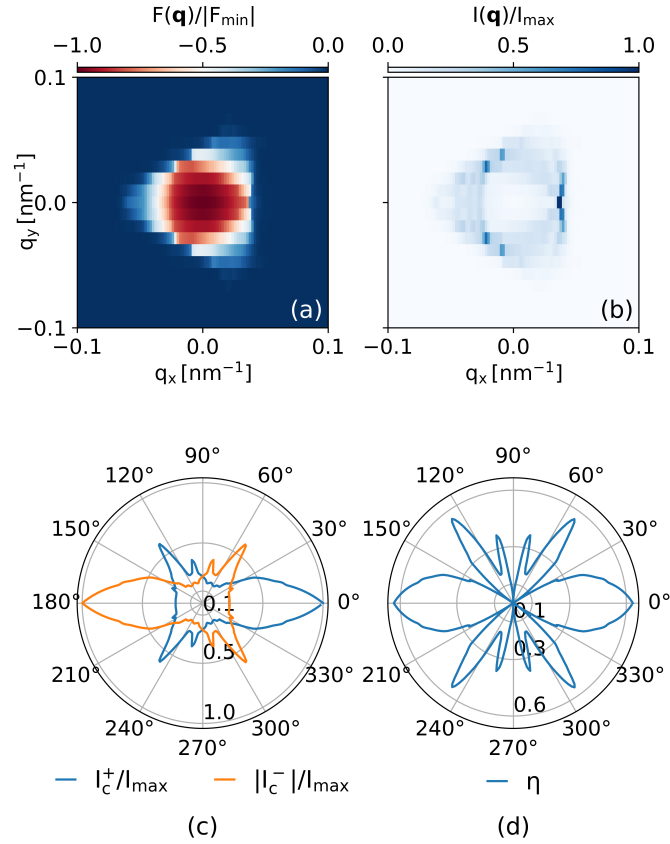


FIG. 6. Results for a Fermi surface with *four connected components* (as shown in Fig. 1(c) of the main text). (a) Free energy, F , as a function of $\mathbf{q} = (q_x, q_y)$. Here, $F_{\min} \equiv \min_{\mathbf{q}} F(\mathbf{q})$. (b) Corresponding supercurrent magnitude, I , as a function of \mathbf{q} . Here, $I_{\max} \equiv \max_{\mathbf{q}} I(\mathbf{q})$. (c) Critical currents in the forward direction ($I_{c,+}$) and reverse direction ($I_{c,-}$) for current direction given by an angle θ relative to the x -direction. (d) Diode efficiency for a current direction given by an angle θ .

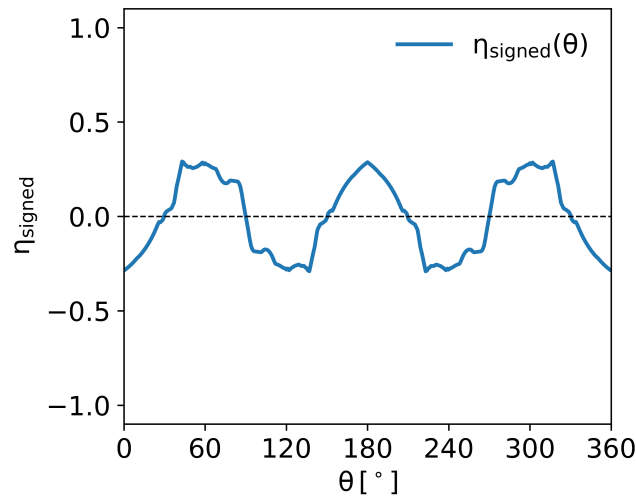


FIG. 7. Signed diode efficiency, η_{signed} as a function of the angle, θ , for the annulus fermi surface discussed in Fig. 3 of the main text.

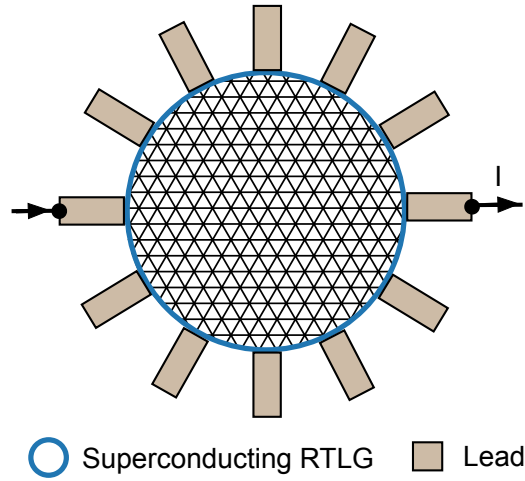


FIG. 8. Possible setup for determining the angular dependence of diode efficiency in RTLQ, inspired by [29]. A circular superconducting RTLQ sample is connected to multiple leads. Application of a current bias, I , along the different directions enables the extraction of the critical currents and diode efficiencies.

2. MEAN-FIELD DECOUPLING

In this second section of the Supplementary Material, we provide a detailed discussion of the mean-field decoupling of the effective interaction Hamiltonian.

We consider only scattering processes of electron pairs with a finite Cooper-pair momentum, \mathbf{q} . Then the effective Hamiltonian of the interacting systems can be written as,

$$H_{\text{eff}} \rightarrow \sum_{\mathbf{k}} \varepsilon_{\mathbf{k}} c_{\mathbf{k}}^{\dagger} c_{\mathbf{k}} + \frac{1}{2\Omega} \sum_{\mathbf{k}, \mathbf{k}', \mathbf{q}} g_{\mathbf{k}, \mathbf{k}', \mathbf{q}} c_{\mathbf{k}+\frac{\mathbf{q}}{2}}^{\dagger} c_{-\mathbf{k}+\frac{\mathbf{q}}{2}}^{\dagger} c_{-\mathbf{k}'+\frac{\mathbf{q}}{2}} c_{\mathbf{k}'+\frac{\mathbf{q}}{2}} \quad (8)$$

with the pairing interaction, $g_{\mathbf{k}, \mathbf{k}', \mathbf{q}} = \tilde{V}_{\mathbf{k}'-\mathbf{k}} F_{\mathbf{k}+\frac{\mathbf{q}}{2}, \mathbf{k}'+\frac{\mathbf{q}}{2}} F_{-\mathbf{k}+\frac{\mathbf{q}}{2}, -\mathbf{k}'+\frac{\mathbf{q}}{2}}$.

Next, we introduce the mean-field,

$$b_{\mathbf{k}', \mathbf{Q}} \equiv \langle c_{-\mathbf{k}'+\frac{\mathbf{q}}{2}} c_{\mathbf{k}'+\frac{\mathbf{q}}{2}} \rangle, \quad (9)$$

which produces the following mean-field Hamiltonian,

$$H_{\text{MF}} = \sum_{\mathbf{k}} \varepsilon_{\mathbf{k}} c_{\mathbf{k}}^{\dagger} c_{\mathbf{k}} - \frac{1}{2} \sum_{\mathbf{k}} \left\{ \Delta_{\mathbf{k}, \mathbf{q}}^* c_{-\mathbf{k}+\frac{\mathbf{q}}{2}} c_{\mathbf{k}+\frac{\mathbf{q}}{2}} + \Delta_{\mathbf{k}, \mathbf{q}} c_{\mathbf{k}+\frac{\mathbf{q}}{2}}^{\dagger} c_{-\mathbf{k}+\frac{\mathbf{q}}{2}}^{\dagger} \right\} + K_{0, \mathbf{q}} \quad (10)$$

with

$$K_{0, \mathbf{q}} = \frac{1}{2} \sum_{\mathbf{k}} \Delta_{\mathbf{k}, \mathbf{q}} b_{\mathbf{k}, \mathbf{q}}^*. \quad (11)$$

In the expression for the mean-field Hamiltonian, we have defined the superconducting order parameter as,

$$\Delta_{\mathbf{k}, \mathbf{q}} = -\frac{1}{\Omega} \sum_{\mathbf{k}'} g_{\mathbf{k}, \mathbf{k}', \mathbf{q}} b_{\mathbf{k}', \mathbf{q}}. \quad (12)$$

We note that $g_{\mathbf{k}, \mathbf{k}', \mathbf{q}} = g_{-\mathbf{k}, -\mathbf{k}', \mathbf{q}}$ and $b_{\mathbf{k}, \mathbf{Q}} = -b_{-\mathbf{k}, \mathbf{Q}}$ from the fermionic anticommutation relations. Hence, the order parameter needs to satisfy,

$$\Delta_{\mathbf{k}, \mathbf{q}} = -\Delta_{-\mathbf{k}, \mathbf{q}}. \quad (13)$$

3. BOGOLIUBOV-DE GENNES HAMILTONIAN

In this third section of the Supplemental Material, we provide details on the derivation of the Bogoliubov-de Gennes Hamiltonian for rhombohedral tetralayer graphene and its diagonalization procedure.

3.1. Hamiltonian formulation

As a starting point, we write down the full system Hamiltonian as,

$$H_{\text{MF},\mathbf{q}} = H_0 + H_\Delta, \quad (14)$$

where H_0 represents the normal-state Hamiltonian and H_Δ is the pairing Hamiltonian.

First, for the normal-state Hamiltonian, we write,

$$\begin{aligned} H_0 &= \sum_{\mathbf{k}} \varepsilon_{\mathbf{k}} c_{\mathbf{k}}^\dagger c_{\mathbf{k}} \\ &= \sum_{\mathbf{k} \in \text{BZ}_+} \varepsilon_{\mathbf{k}+\frac{\mathbf{q}}{2}} c_{\mathbf{k}+\frac{\mathbf{q}}{2}}^\dagger c_{\mathbf{k}+\frac{\mathbf{q}}{2}} + \sum_{\mathbf{k} \in \text{BZ}_+} \varepsilon_{-\mathbf{k}+\frac{\mathbf{q}}{2}} c_{-\mathbf{k}+\frac{\mathbf{q}}{2}} c_{-\mathbf{k}+\frac{\mathbf{q}}{2}}^\dagger + K_{1,\mathbf{q}}, \end{aligned} \quad (15)$$

where the dispersion $\varepsilon_{\mathbf{k}}$ corresponds to the lowest conduction band. In this expression, the Brillouin zone is partitioned as $\text{BZ}_+ \equiv \{\mathbf{k} = (k_x, k_y) \in \text{BZ} \mid k_x > 0\}$ and $\text{BZ}_- \equiv \{\mathbf{k} = (k_x, k_y) \in \text{BZ} \mid k_x < 0\}$. Moreover, the energy offset is defined as

$$K_{1,\mathbf{q}} \equiv \sum_{\mathbf{k} \in \text{BZ}_+} \varepsilon_{-\mathbf{k}+\frac{\mathbf{q}}{2}}. \quad (16)$$

Second, the pairing Hamiltonian is written as

$$\begin{aligned} H_\Delta &= K_{0,\mathbf{q}} - \frac{1}{2} \sum_{\mathbf{k} \in \text{BZ}_+} \left\{ \Delta_{\mathbf{k},\mathbf{q}} c_{\mathbf{k}+\frac{\mathbf{q}}{2}}^\dagger c_{-\mathbf{k}+\frac{\mathbf{q}}{2}}^\dagger + \Delta_{-\mathbf{k},\mathbf{q}} c_{-\mathbf{k}+\frac{\mathbf{q}}{2}}^\dagger c_{\mathbf{k}+\frac{\mathbf{q}}{2}}^\dagger + \text{h.c.} \right\} \\ &= K_{0,\mathbf{q}} - \sum_{\mathbf{k} \in \text{BZ}_+} \left\{ \Delta_{\mathbf{k},\mathbf{q}} c_{\mathbf{k}+\frac{\mathbf{q}}{2}}^\dagger c_{-\mathbf{k}+\frac{\mathbf{q}}{2}}^\dagger + \text{h.c.} \right\}, \end{aligned} \quad (17)$$

Hence, the full Hamiltonian can be written as

$$H = K_{0,\mathbf{q}} + K_{1,\mathbf{q}} + \sum_{\mathbf{k} \in \text{BZ}_+} \Psi_{\mathbf{k},\mathbf{q}}^\dagger \mathcal{H}_{\text{BdG},\mathbf{k},\mathbf{q}} \Psi_{\mathbf{k},\mathbf{q}}, \quad \text{with } \mathcal{H}_{\text{BdG},\mathbf{k},\mathbf{q}} \equiv \begin{pmatrix} \varepsilon_{\mathbf{k}+\frac{\mathbf{q}}{2}} & -\Delta_{\mathbf{k},\mathbf{q}} \\ -\Delta_{\mathbf{k},\mathbf{q}}^* & -\varepsilon_{-\mathbf{k}+\frac{\mathbf{q}}{2}} \end{pmatrix} \quad (18)$$

and the Nambu spinor, $\Psi_{\mathbf{k},\mathbf{q}} \equiv (c_{\mathbf{k}+\frac{\mathbf{q}}{2}}, c_{-\mathbf{k}+\frac{\mathbf{q}}{2}}^\dagger)^T$.

3.2. Hamiltonian Diagonalization

To diagonalize $\mathcal{H}_{\text{BdG},\mathbf{k},\mathbf{q}}$, we first introduce the dispersions

$$\xi_{\mathbf{k},\mathbf{q},\pm} = \frac{\varepsilon_{\mathbf{k}+\frac{\mathbf{q}}{2}} \pm \varepsilon_{-\mathbf{k}+\frac{\mathbf{q}}{2}}}{2}, \quad (19)$$

with $\xi_{\mathbf{k},\mathbf{q},+} = \xi_{-\mathbf{k},\mathbf{q},+}$ and $\xi_{\mathbf{k},\mathbf{q},-} = -\xi_{-\mathbf{k},\mathbf{q},-}$. We can then express the Bogoliubov-de Gennes Hamiltonian as,

$$\mathcal{H}_{\text{BdG},\mathbf{k},\mathbf{q}} = \xi_{\mathbf{k},\mathbf{q},-} \mathbf{I}_{2 \times 2} + \begin{pmatrix} \xi_{\mathbf{k},\mathbf{q},+} & -\Delta_{\mathbf{k},\mathbf{q}} \\ -\Delta_{\mathbf{k},\mathbf{q}}^* & -\xi_{\mathbf{k},\mathbf{q},+} \end{pmatrix}. \quad (20)$$

Next, we define the Bogoliubov transformation

$$\begin{pmatrix} c_{\mathbf{k}+\frac{\mathbf{q}}{2}} \\ c_{-\mathbf{k}+\frac{\mathbf{q}}{2}}^\dagger \end{pmatrix} = W_{\mathbf{k},\mathbf{q}} \begin{pmatrix} \gamma_{\mathbf{k}} \\ \gamma_{-\mathbf{k}}^\dagger \end{pmatrix} \quad \text{with } W_{\mathbf{k},\mathbf{q}} = \begin{pmatrix} u_{\mathbf{k},\mathbf{q}} & e^{i\phi_{\mathbf{k},\mathbf{q}}} v_{\mathbf{k},\mathbf{q}} \\ -e^{-i\phi_{\mathbf{k},\mathbf{q}}} v_{\mathbf{k},\mathbf{q}} & u_{\mathbf{k},\mathbf{q}} \end{pmatrix}. \quad (21)$$

The phase $\phi_{\mathbf{k},\mathbf{q}}$ is defined by $\Delta_{\mathbf{k},\mathbf{q}} = |\Delta_{\mathbf{k},\mathbf{q}}| e^{i\phi_{\mathbf{k},\mathbf{q}}}$. Moreover, the coherence factors are given by

$$\begin{aligned} u_{\mathbf{k},\mathbf{q}}^2 &= \frac{1}{2} \left(1 + \frac{\xi_{\mathbf{k},\mathbf{q},+}}{\sqrt{\xi_{\mathbf{k},\mathbf{q},+}^2 + |\Delta_{\mathbf{k},\mathbf{q}}|^2}} \right), & v_{\mathbf{k},\mathbf{q}}^2 &= \frac{1}{2} \left(1 - \frac{\xi_{\mathbf{k},\mathbf{q},+}}{\sqrt{\xi_{\mathbf{k},\mathbf{q},+}^2 + |\Delta_{\mathbf{k},\mathbf{q}}|^2}} \right), \\ u_{\mathbf{k},\mathbf{q}} v_{\mathbf{k},\mathbf{q}} &= \frac{|\Delta_{\mathbf{k},\mathbf{q}}|}{2\sqrt{\xi_{\mathbf{k},\mathbf{q},+}^2 + |\Delta_{\mathbf{k},\mathbf{q}}|^2}}. \end{aligned} \quad (22)$$

With this transformation, the Bogoliubov-de Gennes Hamiltonian becomes diagonal,

$$W_{\mathbf{k},\mathbf{q}}^\dagger \mathcal{H}_{\text{BdG},\mathbf{k},\mathbf{q}} W_{\mathbf{k},\mathbf{q}} = \begin{pmatrix} E_{\mathbf{k},\mathbf{q},+} & 0 \\ 0 & -E_{\mathbf{k},\mathbf{q},-} \end{pmatrix}, \quad (23)$$

where the energy dispersions are given by

$$E_{\mathbf{k},\mathbf{q},\pm} = \pm \xi_{\mathbf{k},\mathbf{q},-} + \sqrt{\xi_{\mathbf{k},\mathbf{q},+}^2 + |\Delta_{\mathbf{k},\mathbf{q}}|^2}. \quad (24)$$

Moreover, we define,

$$E_{\mathbf{k},\mathbf{q}} \equiv \sqrt{\xi_{\mathbf{k},\mathbf{q},+}^2 + |\Delta_{\mathbf{k},\mathbf{q}}|^2}. \quad (25)$$

The full system Hamiltonian then takes on the diagonalized form

$$\begin{aligned} H &= K_{0,\mathbf{q}} + K_{1,\mathbf{q}} + \sum_{\mathbf{k} \in \text{BZ}_+} [E_{\mathbf{k},\mathbf{q},+} \gamma_{\mathbf{k}}^\dagger \gamma_{\mathbf{k}} - E_{\mathbf{k},\mathbf{q},-} \gamma_{-\mathbf{k}} \gamma_{-\mathbf{k}}^\dagger] \\ &= K_{0,\mathbf{q}} + K_{1,\mathbf{q}} + K_{2,\mathbf{q}} + \sum_{\mathbf{k} \in \text{BZ}_+} [E_{\mathbf{k},\mathbf{q},+} \gamma_{\mathbf{k}}^\dagger \gamma_{\mathbf{k}} + E_{\mathbf{k},\mathbf{q},-} \gamma_{-\mathbf{k}}^\dagger \gamma_{-\mathbf{k}}] \\ &= K_{\mathbf{q}} + \sum_{\mathbf{k} \in \text{BZ}_+} E_{\mathbf{k},\mathbf{q},+} \gamma_{\mathbf{k}}^\dagger \gamma_{\mathbf{k}} + \sum_{\mathbf{k} \in \text{BZ}_-} E_{-\mathbf{k},\mathbf{q},-} \gamma_{\mathbf{k}}^\dagger \gamma_{\mathbf{k}} \\ &= K_{\mathbf{q}} + \sum_{\mathbf{k} \in \text{BZ}_+} E_{\mathbf{k},\mathbf{q},+} \gamma_{\mathbf{k}}^\dagger \gamma_{\mathbf{k}} + \sum_{\mathbf{k} \in \text{BZ}_-} E_{\mathbf{k},\mathbf{q},+} \gamma_{\mathbf{k}}^\dagger \gamma_{\mathbf{k}} \\ &= K_{\mathbf{q}} + \sum_{\mathbf{k} \in \text{BZ}} E_{\mathbf{k},\mathbf{q},+} \gamma_{\mathbf{k}}^\dagger \gamma_{\mathbf{k}}, \end{aligned} \quad (26)$$

where we have used that $E_{\mathbf{k},\mathbf{q},+} = E_{-\mathbf{k},\mathbf{q},-}$, and defined the energy offset

$$K_{2,\mathbf{q}} = - \sum_{\mathbf{k} \in \text{BZ}_+} E_{\mathbf{k},\mathbf{q},-}. \quad (27)$$

The total energy offset is given by

$$\begin{aligned} K_{\mathbf{q}} &= K_{0,\mathbf{q}} + K_{1,\mathbf{q}} + K_{2,\mathbf{q}} \\ &= \sum_{\mathbf{k}} \frac{1}{2} \Delta_{\mathbf{k},\mathbf{q}} b_{\mathbf{k},\mathbf{q}}^* + \sum_{\mathbf{k} \in \text{BZ}_+} \left\{ \varepsilon_{-\mathbf{k}+\frac{\mathbf{q}}{2}} - E_{\mathbf{k},\mathbf{q},-} \right\} \\ &= \sum_{\mathbf{k}} \frac{1}{2} \Delta_{\mathbf{k},\mathbf{q}} b_{\mathbf{k},\mathbf{q}}^* + \frac{1}{2} \sum_{\mathbf{k} \in \text{BZ}} \left\{ \xi_{\mathbf{k},\mathbf{q},+} - E_{\mathbf{k},\mathbf{q}} \right\}. \end{aligned} \quad (28)$$

This completes the formulation and diagonalization of the Bogoliubov-de Gennes Hamiltonian for rhombohedral tetralayer graphene.

4. SELF-CONSISTENCY EQUATION FOR THE SUPERCONDUCTING GAP FUNCTION

In this section of the Supplemental Material, we provide details on the derivation of the self-consistency equation that determines the superconducting gap function.

For this purpose, we need to evaluate the pair correlation function $b_{\mathbf{k},\mathbf{q}} = \langle c_{-\mathbf{k}+\frac{\mathbf{q}}{2}} c_{\mathbf{k}+\frac{\mathbf{q}}{2}} \rangle$.

As a first step, assume that $\mathbf{k} \in \text{BZ}_+$. Then we can write

$$\begin{aligned} c_{-\mathbf{k}+\frac{\mathbf{q}}{2}} c_{\mathbf{k}+\frac{\mathbf{q}}{2}} &= \left\{ -e^{i\phi_{\mathbf{k},\mathbf{q}}} v_{\mathbf{k},\mathbf{q}} \gamma_{\mathbf{k}}^\dagger + u_{\mathbf{k},\mathbf{q}} \gamma_{-\mathbf{k}} \right\} \left\{ u_{\mathbf{k},\mathbf{q}} \gamma_{\mathbf{k}} + e^{i\phi_{\mathbf{k},\mathbf{q}}} v_{\mathbf{k},\mathbf{q}} \gamma_{-\mathbf{k}}^\dagger \right\} \\ &= -e^{i\phi_{\mathbf{k},\mathbf{q}}} v_{\mathbf{k},\mathbf{q}} u_{\mathbf{k},\mathbf{q}} \gamma_{\mathbf{k}}^\dagger \gamma_{\mathbf{k}} - e^{2i\phi_{\mathbf{k},\mathbf{q}}} v_{\mathbf{k},\mathbf{q}}^2 \gamma_{\mathbf{k}}^\dagger \gamma_{-\mathbf{k}}^\dagger + u_{\mathbf{k},\mathbf{q}}^2 \gamma_{-\mathbf{k}} \gamma_{\mathbf{k}} + e^{i\phi_{\mathbf{k},\mathbf{q}}} u_{\mathbf{k},\mathbf{q}} v_{\mathbf{k},\mathbf{q}} \gamma_{-\mathbf{k}} \gamma_{-\mathbf{k}}^\dagger. \end{aligned} \quad (29)$$

Next, we evaluate the following expectation values,

$$\begin{aligned} \langle \gamma_{\mathbf{k}}^\dagger \gamma_{\mathbf{k}} \rangle &= n_F(E_{\mathbf{k},\mathbf{q},+}), \\ \langle \gamma_{-\mathbf{k}} \gamma_{-\mathbf{k}}^\dagger \rangle &= 1 - \langle \gamma_{-\mathbf{k}}^\dagger \gamma_{-\mathbf{k}} \rangle = 1 - n_F(E_{\mathbf{k},\mathbf{q},-}) = 1 - n_F(E_{-\mathbf{k},\mathbf{q},+}), \\ \langle \gamma_{\mathbf{k}}^\dagger \gamma_{-\mathbf{k}}^\dagger \rangle &= 0, \\ \langle \gamma_{-\mathbf{k}} \gamma_{\mathbf{k}} \rangle &= 0. \end{aligned} \quad (30)$$

Here, $n_F(E) \equiv \frac{1}{e^{\beta E} + 1}$ is the Fermi-Dirac distribution function.

Using these results, the pair correlation function becomes

$$\begin{aligned} b_{\mathbf{k},\mathbf{q}} &= e^{i\phi_{\mathbf{k},\mathbf{q}}} u_{\mathbf{k},\mathbf{q}} v_{\mathbf{k},\mathbf{q}} \{1 - n_F(E_{\mathbf{k},\mathbf{q},+}) - n_F(E_{-\mathbf{k},\mathbf{q},+})\} \\ &= \frac{\Delta_{\mathbf{k},\mathbf{q}}}{2E_{\mathbf{k},\mathbf{q}}} \{1 - n_F(E_{\mathbf{k},\mathbf{q},+}) - n_F(E_{-\mathbf{k},\mathbf{q},+})\}. \end{aligned} \quad (31)$$

This result holds for $\mathbf{k} \in \text{BZ}_+$.

As a second step, assume that $\mathbf{k} \in \text{BZ}_-$. Then we can write $\mathbf{k} = -\mathbf{k}'$ for some $\mathbf{k}' \in \text{BZ}_+$. In this case,

$$\begin{aligned} b_{\mathbf{k},\mathbf{q}} &= \langle c_{-\mathbf{k}+\frac{\mathbf{q}}{2}} c_{\mathbf{k}+\frac{\mathbf{q}}{2}} \rangle = \langle c_{\mathbf{k}'+\frac{\mathbf{q}}{2}} c_{-\mathbf{k}'+\frac{\mathbf{q}}{2}} \rangle = -\langle c_{-\mathbf{k}'+\frac{\mathbf{q}}{2}} c_{\mathbf{k}'+\frac{\mathbf{q}}{2}} \rangle = -b_{\mathbf{k}',\mathbf{q}} \\ &= -\frac{\Delta_{\mathbf{k}',\mathbf{q}}}{2E_{\mathbf{k}',\mathbf{q}}} \{1 - n_F(E_{\mathbf{k}',\mathbf{q},+}) - n_F(E_{-\mathbf{k}',\mathbf{q},+})\} \\ &= \frac{\Delta_{\mathbf{k},\mathbf{q}}}{2E_{\mathbf{k},\mathbf{q}}} \{1 - n_F(E_{\mathbf{k},\mathbf{q},+}) - n_F(E_{-\mathbf{k},\mathbf{q},+})\}. \end{aligned} \quad (32)$$

Note that in the first four equalities we are only using the definition of the pair correlation function and the fermionic anti-commutation relations. Only in the fifth equality, we use that $\mathbf{k}' \in \text{BZ}_+$. In the sixth equality, we use the that the superconducting order parameter is an odd function for all $\mathbf{k} \in \text{BZ}$.

Thus, the following expression for the pair correlation function holds for all $\mathbf{k} \in \text{BZ}$,

$$b_{\mathbf{k},\mathbf{q}} = \frac{\Delta_{\mathbf{k},\mathbf{q}}}{2E_{\mathbf{k},\mathbf{q}}} \{1 - n_F(E_{\mathbf{k},\mathbf{q},+}) - n_F(E_{-\mathbf{k},\mathbf{q},+})\}. \quad (33)$$

As a result, the self-consistency gap equation is given by,

$$\begin{aligned} \Delta_{\mathbf{k},\mathbf{q}} &= -\sum_{\mathbf{k}'} g_{\mathbf{k},\mathbf{k}',\mathbf{q}} b_{\mathbf{k}',\mathbf{q}} \\ &= -\sum_{\mathbf{k}'} g_{\mathbf{k},\mathbf{k}',\mathbf{q}} \frac{\Delta_{\mathbf{k}',\mathbf{q}}}{2E_{\mathbf{k}',\mathbf{q}}} \{1 - n_F(E_{\mathbf{k}',\mathbf{q},+}) - n_F(E_{-\mathbf{k}',\mathbf{q},+})\} \\ &= -\sum_{\mathbf{k}'} g_{\mathbf{k},\mathbf{k}',\mathbf{q}} \frac{\Delta_{\mathbf{k}',\mathbf{q}}}{2E_{\mathbf{k}',\mathbf{q}}} \frac{1}{2} \left[\tanh\left(\frac{E_{\mathbf{k}',\mathbf{q},+}}{2k_B T}\right) + \tanh\left(\frac{E_{-\mathbf{k}',\mathbf{q},+}}{2k_B T}\right) \right]. \end{aligned} \quad (34)$$

5. TOTAL ELECTRON DENSITY

In this section of the Supplemental Material, we provide details on the derivation of the total electron density in the superconducting state of the rhombohedral tetralayer graphene system.

In the our mean-field approach to superconductivity, the occupancy of a particular momentum state depends on both the superconducting gap function, $\Delta_{\mathbf{k},\mathbf{Q}}$, and the chemical potential, μ . As a result, the total electron density,

$$n = \frac{1}{\Omega} \sum_{\mathbf{k}} \langle c_{\mathbf{k}}^{\dagger} c_{\mathbf{k}} \rangle. \quad (35)$$

To compute the total electron density, let us write,

$$n = \frac{1}{\Omega} \sum_{\mathbf{k}} \langle c_{\mathbf{k}}^{\dagger} c_{\mathbf{k}} \rangle = \frac{1}{\Omega} \sum_{\mathbf{k}} \langle c_{\mathbf{k}+\frac{\mathbf{q}}{2}}^{\dagger} c_{\mathbf{k}+\frac{\mathbf{q}}{2}} \rangle = \frac{1}{\Omega} \sum_{\mathbf{k} \in \text{BZ}_+} \langle c_{\mathbf{k}+\frac{\mathbf{q}}{2}}^{\dagger} c_{\mathbf{k}+\frac{\mathbf{q}}{2}} \rangle + \frac{1}{\Omega} \sum_{\mathbf{k} \in \text{BZ}_+} \langle c_{-\mathbf{k}+\frac{\mathbf{q}}{2}}^{\dagger} c_{-\mathbf{k}+\frac{\mathbf{q}}{2}} \rangle. \quad (36)$$

For a given $\mathbf{k} \in \text{BZ}_+$, these expectation values are evaluated as,

$$\begin{aligned} \langle c_{\mathbf{k}+\frac{\mathbf{q}}{2}}^{\dagger} c_{\mathbf{k}+\frac{\mathbf{q}}{2}} \rangle &= u_{\mathbf{k},\mathbf{q}}^2 n_F(E_{\mathbf{k},\mathbf{q},+}) - v_{\mathbf{k},\mathbf{q}}^2 n_F(E_{-\mathbf{k},\mathbf{q},+}) + v_{\mathbf{k},\mathbf{q}}^2, \\ \langle c_{-\mathbf{k}+\frac{\mathbf{q}}{2}}^{\dagger} c_{-\mathbf{k}+\frac{\mathbf{q}}{2}} \rangle &= u_{\mathbf{k},\mathbf{q}}^2 n_F(E_{-\mathbf{k},\mathbf{q},+}) - v_{\mathbf{k},\mathbf{q}}^2 n_F(E_{\mathbf{k},\mathbf{q},+}) + v_{\mathbf{k},\mathbf{q}}^2. \end{aligned} \quad (37)$$

Using that $u_{\mathbf{k},\mathbf{q}}^2 = u_{-\mathbf{k},\mathbf{q}}^2$ and $v_{\mathbf{k},\mathbf{q}}^2 = v_{-\mathbf{k},\mathbf{q}}^2$, we obtain the total electron density as

$$n = \frac{1}{\Omega} \sum_{\mathbf{k} \in \text{BZ}} \{ u_{\mathbf{k},\mathbf{q}}^2 n_F(E_{\mathbf{k},\mathbf{q},+}) - v_{\mathbf{k},\mathbf{q}}^2 n_F(E_{-\mathbf{k},\mathbf{q},+}) + v_{\mathbf{k},\mathbf{q}}^2 \}. \quad (38)$$

6. FREE ENERGY

In this section of the Supplemental Material, we provide details on the derivation of the free energy of the rhombohedral tetralayer graphene system.

First, we evaluate the partition function,

$$\begin{aligned} Z &= \text{Tr} [e^{-\beta H}] \\ &= e^{-\beta K_{\mathbf{q}}} \prod_{\mathbf{k} \in \text{BZ}_+} \{1 + e^{-\beta E_{\mathbf{k},\mathbf{q},+}}\} \{1 + e^{-\beta E_{-\mathbf{k},\mathbf{q},+}}\} \\ &= e^{-\beta K_{\mathbf{q}}} \prod_{\mathbf{k} \in \text{BZ}} \{1 + e^{-\beta E_{\mathbf{k},\mathbf{q},+}}\}. \end{aligned} \quad (39)$$

Then the free energy is obtained as,

$$\begin{aligned} \mathcal{F} &= -\frac{1}{\beta} \ln Z \\ &= K_{\mathbf{q}} - \frac{1}{\beta} \sum_{\mathbf{k} \in \text{BZ}_+} \ln [1 + e^{-\beta E_{\mathbf{k},\mathbf{q},+}}] - \frac{1}{\beta} \sum_{\mathbf{k} \in \text{BZ}_+} \ln [1 + e^{-\beta E_{-\mathbf{k},\mathbf{q},+}}] \\ &= K_{\mathbf{q}} - \frac{1}{\beta} \sum_{\mathbf{k} \in \text{BZ}} \ln [1 + e^{-\beta E_{\mathbf{k},\mathbf{q},+}}]. \end{aligned} \quad (40)$$

For convenience, let us write down again the energy offset,

$$K_{\mathbf{q}} = \sum_{\mathbf{k}} \frac{1}{2} \Delta_{\mathbf{k},\mathbf{q}} b_{\mathbf{k},\mathbf{q}}^* + \frac{1}{2} \sum_{\mathbf{k}} \{ \xi_{\mathbf{k},\mathbf{q},+} - E_{\mathbf{k},\mathbf{q}} \} \quad (41)$$

where

$$b_{\mathbf{k},\mathbf{q}} = \frac{\Delta_{\mathbf{k},\mathbf{q}}}{2E_{\mathbf{k},\mathbf{q}}} \{1 - n_F(E_{\mathbf{k},\mathbf{q},+}) - n_F(E_{-\mathbf{k},\mathbf{q},+})\}. \quad (42)$$